Materials Science and Engineering C 31 (2011) 775–780

Contents lists available at ScienceDirect

Materials Science and Engineering C

journal homepage: www.elsevier.com/locate/msec

Triangular core as a universal strategy for stiff nanostructures in biology and biologically inspired materials

Sinan Keten [a,b], Zhiping Xu [a], Markus J. Buehler [a,*]

[a] Laboratory for Atomistic and Molecular Mechanics, Department of Civil and Environmental Engineering, Massachusetts Institute of Technology, 77 Massachusetts Ave. Room 1-235A&B, Cambridge, MA, USA

[b] Department of Civil & Environmental Engineering and Mechanical Engineering, 2145 Sheridan Road, Northwestern University, Evanston, Illinois 60208-3109, USA

ARTICLE INFO

Article history:
Received 16 March 2010
Received in revised form 21 December 2010
Accepted 11 January 2011
Available online 19 January 2011

Keywords:
Mechanical properties
Structure
Cross-section
Biomechanics
Materiomics
Deformation
Stiffness
Persistence length
Nanostructure

ABSTRACT

Recent findings in protein structure prediction have revealed a new class of fibrous proteins called beta-solenoids. In stark resemblance to amyloid structures and prion proteins, these self-assembling peptides feature a triangular cross-sectional structure with non-specific biological significance. Using basic geometric and mechanical arguments and finite element simulations, here we point out that the equilateral triangle, as the most anisotropic regular convex polytope, is an ideal shape that leads to a maximum bending stiffness at minimum material usage. Considering the mechanical stability of the cell-puncture needle of the bacteriophage T4 virus and the extreme efficiency of aggregation in amyloids and prion proteins, possibly due to their capacity of acting as rigid binding and nucleation sites, we propose that the triangular core may reflect a universal biological paradigm for achieving exceptionally stiff nanostructures, overcoming the limitations of the underlying weak molecular interactions such as hydrogen bonds. Stiff nanostructures employing a triangular core geometry may be particularly useful for nanomechanical applications such as puncture and cutting devices where maximum rigidity has to be achieved using a minimal cross-sectional area.

1. Introduction

Recent advances in protein structure prediction techniques such as solid-state nuclear magnetic resonance (ssNMR) [1–3] have yielded detailed insight into the molecular architecture of fibrous protein oligomers with sub nano-scale precision, revealing a universal motif that features a triangular shaped core for these self-assembling peptides. Some of these protein structures have physiological functions in biology, whereas others occur spontaneously as a result of prion diseases. Certain amyloid fibrils that are found in Alzheimer's Disease also employ a triangular core with 3-fold symmetry [4] (Fig. 1(a)). Experimental evidence suggests that amyloid filaments are stiff, resulting in a large bending rigidity [5]. The interaction of these relatively rigid filaments with the surrounding cells and extracellular matrix may cause mechanical disruption of tissue and play a role in pathological pathways of diseases [6,7].

Similarly, beta-solenoids, a recently discovered class of protein topologies with triangular cross-sections, have been linked to pathological building blocks of prion diseases as well as virulence factors [8,9]. The high mechanical stiffness is utilized in biology as part of viral infection mechanisms. For example, the cell-puncture device needle of the bacteriophage T4 virus, a beta-solenoid with a triangular core [10], has been identified as a stiff needle that facilitates the drilling through the cell membrane of bacteria as part of the infection process [11] (Fig. 1(b)). At the macroscale, twisted triangular cross-sections are used in high-rise buildings as they have lower drag coefficients and reduce service loads due to wind. Triangular lattice structures have been also been used commonly at the macroscale in structural engineering for their inherent lateral stability. A similar effect can be expected in biological systems where shear forces due to fluid flow would be reduced in twisted triangular filaments, leading to higher effective rigidity.

2. Results and discussion

The central matter addressed in this article is whether the triangulation of the core may be a universal strategy to create structures with minimal amount of material use, yet maximum rigidity. To answer this question, we divert the reader's attention to a centuries old problem in mechanics: the shape of the strongest column, or posing the question in the terminology of biology, the shape of the strongest filament. Lagrange, Weinberger, Clausen and others have studied this fundamental problem; and several solution approaches have been discussed controversially for the selection of the optimal cross-sectional shape [12,13]. Here we simplify the analysis to emphasize the biological and nanomechanics relevance, and consider a select number of convex

* Corresponding author. Tel.: +1 617 452 2750.
E-mail address: mbuehler@MIT.EDU (M.J. Buehler).

0928-4931/$ – see front matter © 2011 Elsevier B.V. All rights reserved.
doi:10.1016/j.msec.2011.01.004

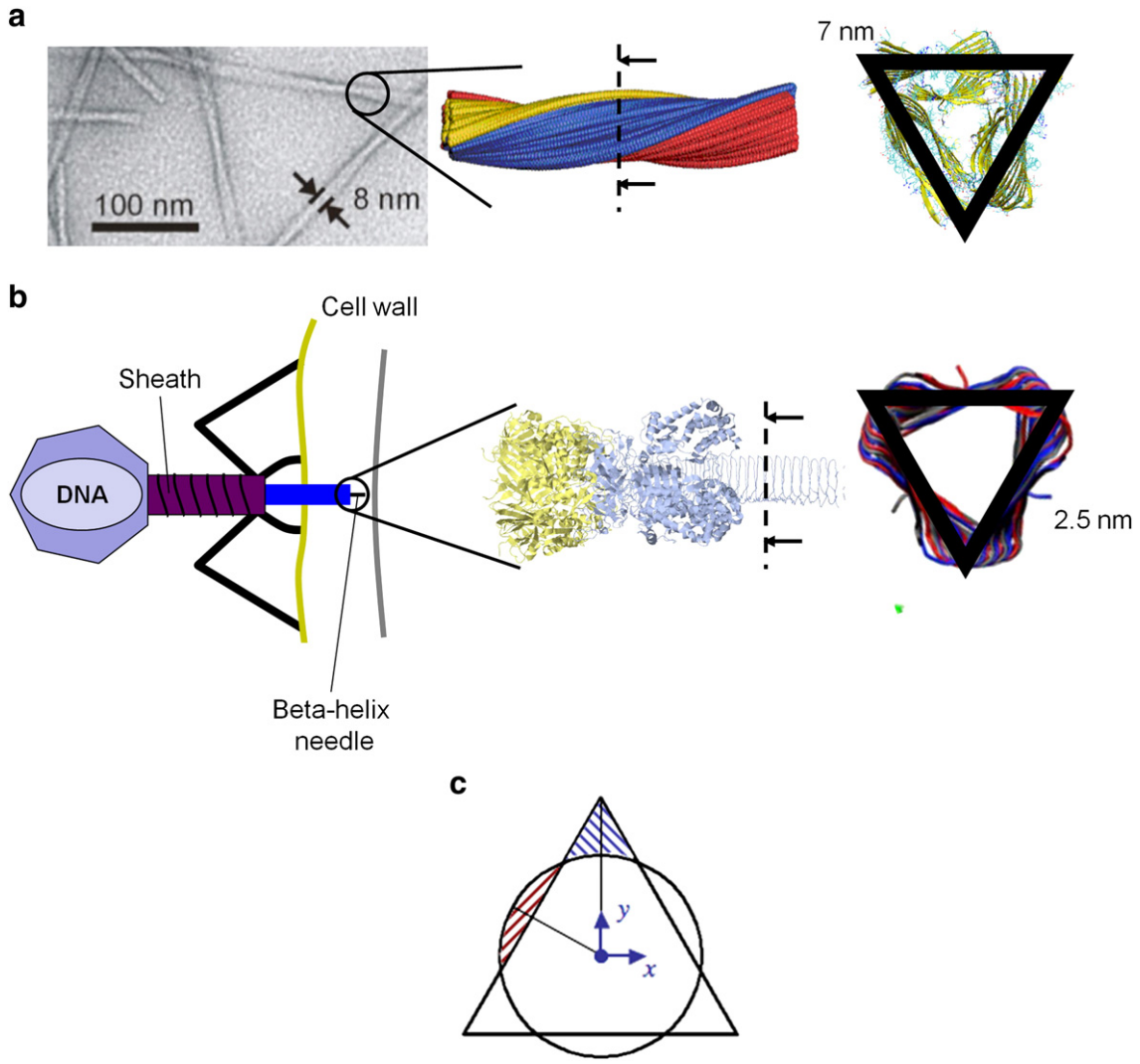

Fig. 1. Triangular core of amyloids and beta-solenoids. The figure illustrates the cross-sectional properties of triangular peptide nanostructures discussed here. Side-chain atoms occupying the core are not shown in the simple cartoon representation. An equilateral triangle has been proposed as the cross-sectional shape of the 3-cross structure of certain amyloids in Alzheimer's Disease (a). Cell-puncture device needle of bacteriophage T4 virus (b) is triple beta-helix with an equilateral triangle as the cross section. For the amyloids, each side is approximately 7 nm in length, whereas the cell-puncture device needle is much smaller, with a side length of approximately 2.5 nm. Panel (c) illustrates triangular and circular cross-sections of identical area. Axes indicated could be used to calculate second moment of area, which is defined for instance for the x-axis as $I_{xx} = \int x^2 dA$ (similarly, for the y-axis $I_{yy} = \int y^2 dA$). Due to the symmetry of the structures, I is the same along any axis passing through the centroid, but larger for the triangle than for the circle. Comparing the shaded areas that lie outside the shared region, one can easily see that the triangular cross section places more area away from the centroid, thereby dramatically increasing I for the same amount of material. We observe that approximately 21% increase in bending rigidity can be achieved by triangulation. Panel (a, left) modified from Paravustu *et al.*, PNAS, 2008 [4], copyright © 2008 National Academy of Sciences, USA.

cross-sections observed in biological and engineering structures. We build on the previous theoretical derivations to put the results into the context of experimental techniques available to study filaments at the nano-scale. In particular, we discuss the variation of bending rigidity and shear effects as a function of length and their influence on experimental measurements. We conclude the discussion by considering a variety of relevant triangular cross-sections in biological protein materials and emphasize the suitability of this shape for creating stiff, stable nanostructures that could efficiently perform biomechanical functions.

The bending rigidity of a filament is linked to geometrical features of its cross-section such as the second moment of area (I) and the cross-sectional area (A). For a filament of given cross sectional area A, and length L, the ability to resist bending due to thermal or mechanical forces is directly proportional to EI, where E denotes elastic modulus of the material obtained by measuring the relationship between force and elongation in a tensile stretching test. For a given filament length and material properties (i.e., elastic modulus, E), the radius of gyration defined as $r_G = \sqrt{I_{min}/A}$, provides a measure of a cross-section's capacity to resist bending, where $I_{\min}$ denotes the smallest second moment of area along any axis passing through the centroid of the cross-section. This axis is the weakest axis along which bending or buckling of the structure would be easier under ambient forces. As such, the parameter r_G is commonly used in structural mechanics as a key parameter for quantifying the failure strength of columns in buildings. Similarly, r_G is also used in polymer science to quantify the flexibility of a macromolecule, and is linked to the persistence length, representing the length beyond which direction vectors of a filament are uncorrelated. Persistence length is directly correlated to bending rigidity as $\xi_P = \frac{EI}{k_B T}$. Persistence lengths of different classes of biological filaments are given in Table 1. We note that while the scatter is large, an intriguing observation is that biological structures with triangular cross-sections (e.g. beta-helices) tend to have relatively higher persistence lengths than structures with comparable diameter (e.g. tropocollagen or intermediate filaments), providing evidence for the mechanical efficiency of these structures. This is directly visualized in Fig. 2, which shows a plot of persistence length over filament diameter.

Table 1
Diameter (d) and persistence length (ξ_P) values for single biological molecules and biomolecular assemblies.

Biological molecule	d (nm)	ξ_P (nm)	Ref.
Polypeptide chain	0.5	0.4	[20,21]
Tropocollagen	2	11-16	[22,23]
Actin filament	6–8	3000–17,000	[24,25]
Intermediate filament	10	1000–3000	[25]
Single beta-helix[a]	3	900–1400	[26]
Triple beta-helix[a]	3	800–14,000	[11]
Amyloid[a,b]	4-7	6,000–50,000	[18,27]
Microtubule	25	1,000,000–8,000,000	[24]

[a] Triangular cross-section.
[b] Not all amyloid filaments feature a triangular cross-section.

The second moment of area, I around an axis is defined as $I_{xx} = \int x^2 dA$. For the equilateral triangle, second moment of area is the same for all axes passing through the centroid and is given as [14]:

$$I_{xx} = I_{yy} = \frac{bh^3}{36} = \frac{hb^3}{48}. \quad (1)$$

In this case, the minimum second moment of area is given as:

$$I^{\Delta}_{min} = \frac{\sqrt{3}b^4}{96} \quad (2)$$

where b denotes the length of a side. For a circle, second moment of area is again the same for all axes passing through the centroid and is given as [14]:

$$I_{xx} = I_{yy} = \frac{\pi r^4}{4} \quad (3)$$

Considering an area (and for constant length, volume) equality, one can evaluate the minimum moment of area of a circle as:

$$I^{O}_{min} = \frac{3b^4}{64\pi} \quad (4)$$

One can then compute the ratio $I^{\Delta}_{\min}/I^{O}_{\min}$ to compare which section for given cross-sectional area, A, yields higher minimum second moment of inertia. In this case, we observe that the triangle beats the circle by 21%. In typical Euler buckling formula for columns, failure load is directly related to $I_{\min}$ such that:

$$P_{cr} \sim I_{min}/A \sim r_G \quad (5)$$

where r_G is the radius of gyration. Hence by maximizing $I_{\min}$, a triangular column makes use of material in a better fashion to yield stiffer structures. The argument is also valid for overall bending rigidity, leading to more persistent fibers. One can also show that the same reasoning applies for hollow sections provided that the wall thickness is large enough to prevent shell buckling.

The cross sections of circle or regular convex polytopes discussed above, such as equilateral triangle, square and hexagon, have the advantage that the rigidities for bending in different planes containing the axis are the same. For other shapes like rectangle with disparate length and width, the bending resistance is then limited by the mode with lower rigidity.

Based on continuum analysis, we also point out that filaments with an equilateral triangle as the cross-section have the greatest radius of gyration (see also Materials and Methods) than any other convex cross-sectional shape for a constant cross-sectional area, including a circle. The advantage of the triangle that leads to 21% higher rigidity is its capability of distributing material further from the principal axes, away from the center, to provide a more efficient resistance to bending. Fig. 1(c) illustrates this concept by highlighting difference in the cross-sectional distribution of a triangle and a circle with equal areas.

Having illustrated the basic underlying physics of the superior performance of a triangle, we extend this analysis by studying the length-dependent bending properties of biological filaments. The motivation here is to understand the influence of length on the effective rigidity of filaments that have cross-sectional shapes. Here we consider five cross-sections, triangle, square, hexagon, circle and triangle with rounded corners (considering that the corresponding biological structures with a sharp corner would have too high potential energy), all with equal area. We note that estimating the exact continuum equivalent corner radius from experimental data is quite challenging due to the discontinuous nature of the corners in amyloids, and the flexible, bulged nature of these sections in beta-helices. Therefore, we use a straight edges and circular corners with continuous tangents for developing the rounded triangle geometry. We find that a rounded corner with a finite radius of curvature lowers the bending moment of inertia due to the loss of anisotropy. The radius of curvature of the corner increases from zero in the triangle case to a finite value, for which the maximum value for a given cross-sectional area constitutes the circle scenario.

Fig. 3(a) shows the structures investigated in this study. For long filaments, pure bending equations of an Euler–Bernoulli beam are used commonly to extract mechanical properties such as Young's modulus from force-spectroscopy experiments, which test finite length filaments in bending. Our goal here is to investigate the length at which the simple Euler–Bernoulli formulation breaks down and instead the Timoshenko beam formula, which considers shear and rotation effects, needs to be used for each cross-section. Fig. 3(b) illustrates this concept; as the length of the filaments is reduced, shear effects become more important and the bending rigidity $D_B = EI$ that would be computed using pure bending assumption deviates from the actual bending rigidity of the filament, D. The critical length scale at which this transition occurs is around 25 nm for structures with an effective diameter of 1 nm and Poisson's ratio of $\nu = 0.33$. Noting that biomolecular structures are typically highly anisotropic and can have effective Poisson's ratios greater than 1 at low shear modulus $G = E/2(1+\nu)$ values, we anticipate that this length scale can be larger for some biological structures. Indeed, this is supported by recent experimental studies on microtubules, which showed significant contributions from shear deformation [15]. Further, the triangle

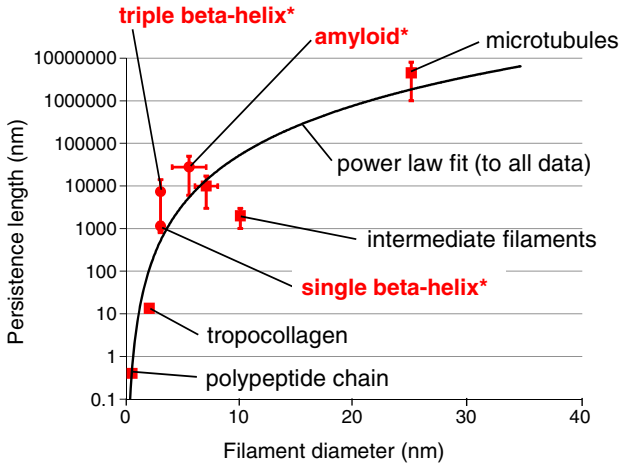

Fig. 2. Plot of persistence length (ξ_P) over diameter (d) for single biological molecules and biomolecular assemblies. The analysis provides some evidence that biological structures with triangular cross-sections (marked with *) tend to have relatively higher persistence lengths than structures with comparable diameter (e.g. tropocollagen or intermediate filaments), providing evidence for the mechanical efficiency of these structures. Plot based on the data shown in Table 1.

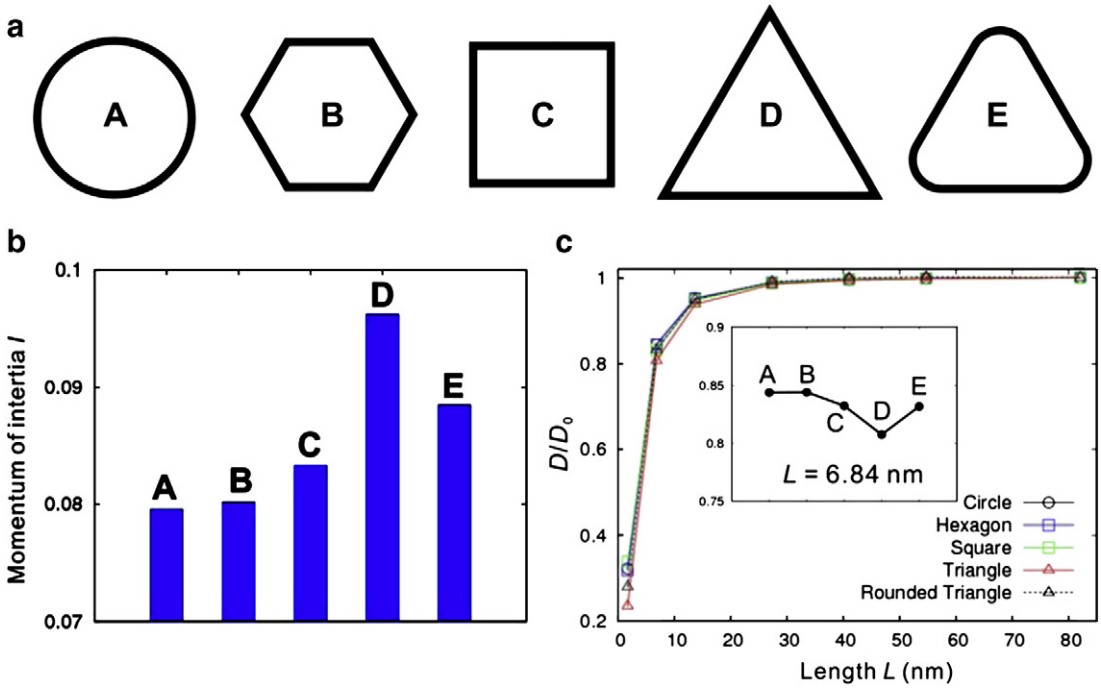

Fig. 3. Mechanical rigidity of filaments with various cross-sectional geometries. Panel (a) illustrates the shapes studied in this paper. Panel (b) shows the moment of inertia of various cross-sections, with triangle providing 21% higher rigidity than a circle with the same area. The moment of inertia I is in quartic length units. Panel (c) shows results from finite element simulations, where the effect of shear is quantified as the system length is varied. When the length is smaller than a critical transition value, shear contribution to deformation is very important, hence the bending rigidity D of the system observed from experiments can be different from the actual. As the length of the filament is increased, the results converge to Euler-Bernoulli behavior ($D = D_B$). The inset shows relative values of D/D_B at fibril length $L = 6.84$ nm.

has the highest anisotropy in the cross sections we discussed. This implies that triangle will have the most significant effect of shear contribution and therefore the largest critical length scale below which these effects should be considered, as shown in the inset of Fig. 3(c). Fig. 4 shows results of a finite element analysis of the geometry with the ideal cross-section, where panel (a) illustrates the loading condition, where a cantilever with a constant load at the free end is considered. Fig. 4(b) shows the shear strains in the structure for different lengths, illustrating the transition from shear governed mechanics to bending governed deformation.

3. Discussion and conclusion

The analysis presented here applies continuum modeling to assess the bending rigidity of common cross-sectional shapes found in biological filaments. These findings are scale-independent and universal since they are purely geometrical, and can in principle be significant at all length-scales, including nanostructures. The twisted triangular core of the cell-puncture needle, as well as amyloid filaments and many other fibrous protein topologies [16] may suggest that this concept also emerges as a design principle in biology, be it as a result of spontaneous aggregation as in amyloids, or as part of an evolutionary strategy as in the case of T4 virus. An investigation of the mechanical properties of these biological nanofibers merits further studies that focus on the universal geometric features of these structures and their link to their mechanical properties. Atomistic simulations can shed light on further mechanisms that arise at the nanoscale. For instance, surface effects, hydrophobic interactions and defect-free H-bond networks can contribute further to mechanical properties and failure phenomena in biological systems. Similarly, rigidity of larger structures and biological assemblies will depend on defects and inhomogeneities that govern the behavior beyond the micrometer scale. Ideas that build on the basic geometrical principles presented in this study, in conjunction with multi-scale modeling approaches, could facilitate efficient designs inspired from biology, providing a merger of materials and structures that lead to superior mechanical properties such as exceptional rigidity and strength [17].

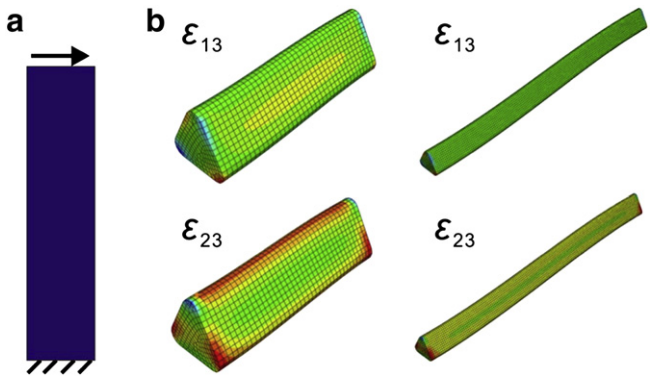

Fig. 4. Finite element analysis of the geometry with the ideal cross-section. Panel (a) illustrates the loading condition, where a cantilever with a constant load at the free end is considered. Panel (b) shows the shear strains in the structure for different lengths, illustrating the transition from shear governed mechanics to bending governed deformation.

4. Materials and methods

4.1. Comparison of circle and triangle as ideal cross-sections

Here we describe the basic underlying theoretical principles underlying the projection that triangle is an ideal shape for achieving higher stiffness for a material of given length and area (constant volume). In this simplified proof, the variation of the cross-section (i.e., tapering), twist and other effects are neglected, and only comparison with a circle is given.

We begin with an area equality criterion that gives corresponding dimensions for circle and triangle:

$$\pi r^2 \equiv \frac{bh}{2} \tag{6}$$

where b, h denote the base and height of the equilateral triangle, and r is the radius of the circle with equivalent area. For an equilateral triangle,

$$h = \frac{\sqrt{3}b}{2} \tag{7}$$

and therefore the equivalence in Eq. (6) becomes :

$$r^2 = \frac{\sqrt{3}b^2}{4\pi} \tag{8}$$

The second moment of area, I around an axis is defined as $I_{xx} = \int x^2 dA$. For the equilateral triangle, second moment of area is the same for all axes passing through the centroid and is given as [14]:

$$I_{xx} = I_{yy} = \frac{bh^3}{36} = \frac{hb^3}{48}. \tag{9}$$

In this case, the minimum second moment of area is given as:

$$I^{\Delta}_{min} = \frac{\sqrt{3}b^4}{96} \tag{10}$$

where b denotes the length of a side. For a circle, second moment of area is again the same for all axes passing through the centroid and is given as [14]:

$$I_{xx} = I_{yy} = \frac{\pi r^4}{4} \tag{11}$$

Recalling Eq. (8), the area (and for constant length, volume) equality, one can evaluate the minimum moment of area as :

$$I^{O}_{min} = \frac{3b^4}{64\pi} \tag{12}$$

One can then compute the ratio $I^{\Delta}_{\min}/I^{O}_{\min}$ to compare which section for given cross-sectional area, A, yields higher minimum second moment of inertia. In this case, we observe that the triangle beats the circle by 21%. In typical Euler buckling formula for columns, failure load is directly related to $I_{\min}$ such that:

$$P_{cr} \sim I_{min}/A \sim \rho^2 \tag{13}$$

where $\rho = \sqrt{\frac{I_{min}}{A}}$ is the radius of gyration. Hence by maximizing $I_{\min}$, a triangular column makes use of material in a better fashion to yield stiffer structures. The argument is also valid for overall bending rigidity, leading to more persistent fibers. One can also show that the same reasoning applies for hollow sections provided that the wall thickness is large enough to prevent shell buckling.

4.2. Finite element simulations

Finite element analysis is carried out using three-dimensional element C3D8. The material is isotropic with Young's modulus E and Poisson's ratio $\nu = 1/3$. The Poisson's ratio from previous studies on biological materials has shown that it exceeds 1, which violates thermodynamics constraint on the isotropic elastic constants, and thus a value of 1/3 is used here. As a result, the elastic properties of the material is determined by a single parameter E. For simplicity, we use $E = 1$ in the simulation and the amplitude of stress, if needed, could be obtained by renormalization according to the physical Young's modulus (values for E from atomistic simulation could be taken, e.g. ≈18 GPa as recently reported for amyloid fibrils [18]). For the same reason, the mass density of the material and its length scale are also scaled.

For beams with cross sections shown in Fig. 3, a first-order eigenmode analysis is performed with free-end boundary conditions. The effective bending rigidity D is obtained from simulations, where the vibrational frequency is given as:

$$w = k^2\sqrt{\frac{D}{\rho A}},\ k = \frac{C_1}{L}, \tag{14}$$

and the effective bending rigidity is

$$D(L) = \rho A w^2 / k^4. \tag{15}$$

Here L is the length of the beam, ρ is the mass density, and numeric constant $C_1 = 4.73$. Euler–Bernoulli beam model fails when the aspect ratio is low, thus from Eq. 15 we know that for beams that are sufficiently long, $D = D_B$ and is constant. For short beams, $D = D(L)$ calculated from Eq. (15) will depend on the fibril length because of the shear and rotation contributions [19]. In these cases, the Timoshenko beam model is applied.

Acknowledgements

This work was supported by the Office of Naval Research (N00014-08-1-00844), with additional support from the Air Force Office of Scientific Research, Army Research Office, DARPA, MITEI and the National Science Foundation.

References

[1] A.T. Petkova, Y. Ishii, J.J. Balbach, O.N. Anzutkin, R.D. Leapman, F. Delaglio, R. Tycko, Proceedings of the National Academy of Sciences of the United States of America 99 (2002) 16742–16747.
[2] C.P. Jaroniec, C.E. MacPhee, N.S. Astrof, C.M. Dobson, R.G. Griffin, Proceedings of the National Academy of Sciences of the United States of America 99 (2004) 16748–16753.
[3] A. Paravastu, R.D. Leapman, W.-M. Yau, R. Tycko, Proceedings of the National Academy of Sciences of the United States of America 105 (2008) 18349–18354.
[4] A.K. Paravastu, R.D. Leapman, W.M. Yau, R. Tycko, Proceedings of the National Academy of Sciences of the United States of America 105 (2008) 18349–18354.
[5] T.P. Knowles, A.W. Fitzpatrick, S. Meehan, H.R. Mott, M. Vendruscolo, C.M. Dobson, M.E. Welland, Science 318 (2007) 1900–1903.
[6] K.B. Shah, Y. Inoue, M.R. Mehra, Archives of Internal Medicine 166 (2006) 1805–1813.
[7] M.J. Buehler, Y.C. Yung, Nature Materials 8 (2009) 175–188.
[8] A. Kajava, J. Squire, D. Parry, Fibrous Proteins: Amyloids, Prions and Beta Proteins 73 (2006) 1-+.
[9] C. Wasmer, A. Lange, H. Van Melckebeke, A. Siemer, R. Riek, B. Meier, Science 319 (2008) 1523–1526.
[10] S. Kanamaru, P.G. Leiman, V.A. Kostyuchenko, P.R. Chipman, V.V. Mesyanzhinov, F. Arisaka, M.G. Rossmann, Nature 415 (2002) 553–557.
[11] S. Keten, J. Rodriguez Alvarado, S. Müftü, M. Buehler, Cellular and Molecular Bioengineering 2 (2009) 66–74.
[12] X.D. Li, P. Nardi, C.W. Baek, J.M. Kim, Y.K. Kim, Journal of Micromechanics and Microengineering 15 (2005) 551–556.
[13] J. Keller, Archive for Rational Mechanics and Analysis 5 (1960) 275–285.
[14] J.M. Gere, Mechanics of materials, Brooks/Cole, Belmont, Calif., 2004, p. 940.
[15] F. Pampaloni, G. Lattanzi, A. Jonas, T. Surrey, E. Frey, E.L. Florin, Proceedings of the National Academy of Sciences of the United States of America 103 (2006) 10248–10253.
[16] M. Upmanyu, H.L. Wang, H.Y. Liang, R. Mahajan, Journal of the Royal Society, Interface 5 (2008) 303–310.
[17] H.D. Espinosa, J.E. Rim, F. Barthelat, M.J. Buehler, Progress in Materials Science 54 (2009) 1059–1100.
[18] R. Paparcone, S. Keten, M.J. Buehler, Journal of Biomechanics 43 (2010) 1196–1201.
[19] W.J. Weaver, S.P. Timoshenko, D.H. Young, Vibration Problems in Engineering, Wiley-Interscience, Hoboken, NJ, 2001.
[20] M. Rief, M. Gautel, F. Oesterhelt, J.M. Fernandez, H.E. Gaub, Science 276 (1997) 1109–1112.
[21] E. Oroudjev, J. Soares, S. Arcidiacono, J.B. Thompson, S.A. Fossey, H.G. Hansma, Proceedings of the National Academy of Sciences of the United States of America 99 (2002) 6460–6465.

[22] Y.L. Sun, Z.P. Luo, A. Fertala, K.N. An, Biochemical and Biophysical Research Communications 295 (2002) 382–386.
[23] M. Buehler, S. Wong, Biophysical Journal 93 (2007) 37–43.
[24] F. Gittes, B. Mickey, J. Nettleton, J. Howard, The Journal of Cell Biology 120 (1993) 923–934.
[25] N. Mucke, L. Kreplak, R. Kirmse, T. Wedig, H. Herrmann, U. Aebi, J. Langowski, Journal of Molecular Biology 335 (2004) 1241–1250.
[26] S. Keten, M.J. Buehler, Computer Methods in Applied Mechanics and Engineering 197 (2008) 3203–3214.
[27] J.F. Smith, T.P.J. Knowles, C.M. Dobson, C.E. MacPhee, M.E. Welland, Proceedings of the National Academy of Sciences of the United States of America 103 (2006) 15806–15811.